Proceedings Paper:
Lockwood, APG, Warren, NJ, Peakall, J orcid.org/0000-0003-3382-4578 et al. (5 more authors) (2021) A Comparison of the Sedimentation Dynamics of Statistical and Diblock Copolymer Flocculation Aids in Radwaste Dewatering. In: Waste Management Symposium. Online, 08-12 Mar 2021, Online. .

A Comparison of the Sedimentation Dynamics of Statistical and Diblock Copolymer Flocculation Aids in Radwaste Dewatering - 21298

Alexander P. G. Lockwood[1], Nicholas J. Warren[1], Jeffrey Peakall[2], Serish Hussain[1], Geoff Randall[3], Martyn G. Barnes[3], David Harbottle[1], Timothy N. Hunter[1]

1. School of Chemical and Process Engineering, University of Leeds, LS2 9JT, United Kingdom
2. School of Earth and Environment, University of Leeds, LS2 9JT, United Kingdom
3. Centre of Sludge Expertise, Sellafield Ltd, Birchwood, WA3 6GR

ABSTRACT

Polymeric flocculation is of significant interest to nuclear waste management operations. Particularly in early storage ponds, where first-generation fuel designs were placed for cooling before reprocessing. The prolonged storage of these fuels has led to subsequent fuel cladding corrosion. Sites where this corrosion has occurred, such as the USA Hanford site K Basin and the First-Generation Magnox Storage Pond (FGMSP) at the Sellafield site in the UK, have faced significant challenges from the resultant hydroxide-based sludges, mainly from slow setting and colloidal particulates. As these particulates have a slight cationic surface charge, anionic polymer flocculation agents have previously been deployed to aid sedimentation of these particles. Traditionally, water treatment industries opt for low charge density (30%-40% anionic strength) statistical copolymers, which have a random configuration of anionic to non-ionic monomers to achieve the required charge density and are usually in the order of 10^5-10^7 g.mol^{-1} molecular weight. These polymers adsorb to cationic particle surfaces, but due to their slow surface conformation kinetics, possess a residual polymer chain length in the form of 'loops' and 'tails', which expand out into solution past the electrical double layer stability region (Debye length) of the particulates, allowing them to bind to adjacent particles in suspension. This 'bridging' flocculation mechanism creates large open and porous structures which have superior sedimentation dynamics to the initial suspension. Other flocculation mechanisms have been investigated, such as "charge patch" flocculation, which uses smaller (10^4-10^5 g.mol^{-1}) polymers of 80-100% charge densities to adsorb denser and flatter onto a particles surface, resulting in localised charge reversal allowing particles to electrostatically bind. This mechanism conversely produces smaller but denser flocs than bridging flocculation. Hindered sedimentation is complex and depending on the system parameters, such as particle concentration, one flocculation mechanism may be more beneficial than another. Bridging flocculation systems generally sediment faster, but due to their open structures and electrostatic repulsion of adjacent anionic functional groups in the polymer, produce larger, less dense bed volumes, which are less ideal for final storage and disposal. Additionally, there has been increasing interest in flotation as a dewatering mechanism, specifically using diblock copolymers, which act as dual collector and flocculation agents to target finer particulates in the flotation stage and in subsequent thickening processes, sediment coarser particles. Unlike the statistical copolymers in bridging flocculation, diblock polymers have segregated anionic and non-ionic regions, making them amphiphilic and surface active like surfactants. As the anionic segment is highly charged, these systems utilise a "charge patch" flocculation mechanism. However, during bed consolidation, the corona of highly hydrophobic non-ionic chains may provide an additional entropic driving force to complement compressive forces to further dewater the floc bed, producing more compact waste forms. This investigation compares the sedimentation rates, floc structures and final bed volumes of sedimented $Mg(OH)_2$ using both statistical and diblock copolymers.

INTRODUCTION

The first generation of Brittish civil nuclear power was delivered by the Magnox fleet of gas cooled nuclear power reactors constructed in the 1950s. Named after the alloy which their cladding was constructed from (an alloy of primarily magnesium, 0.7% aluminium and 5ppm beryllium)[1], this fuel was stored in a bespoke outdoor water cooling facility, the first generation Magnox storage pond (FGMSP), until the fuel could be reprocessed. However, due to the open-air nature of the facility, the spent Magnox clad fuel has been subject to external contaminants, resulting in a restricted ability to control pond water chemistry[2]. This poor water chemistry control combined with the extended storage period, has resulted in the extensive corrosion of the Magnox cladding, resulting in a large inventory of corroded sludge and suspended particulates in FGMSP estimated to be ~1300 m^3 illustrated in Fig. 1[3]. The corrosion process has released radionuclides from the spent fuel raising activity levels in pond water to ~1000 $TBq.m^{-3}$ [4]. The corrosion process has additionally led to the production of $Mg(OH)_2$ colloidal material. Maher et al.[5] found that $Mg(OH)_2$ colloidal brucite is a potential controller of radionuclide speciation, capable of incorporating radionuclides (particularly the actinides) into their structure such as Pu^{5+} and Am^{3+}. The downstream site ion exchange effluent plant (SIXEP) poorly abates these radionuclides, thus a reduction in the transport of $Mg(OH)_2$ particulates to SIXEP to prevent this contamination vector is crucial to reducing high alpha activity effluents[6]. Additionally, the presence of $Mg(OH)_2$ reduces the performance of SIXEP, with Mg^{2+} ions competing with $^{137}Cs^{+}$ and $^{90}Sr^{2+}$ for ion exchange sites on the clinoptilolite ion exchange media[7].

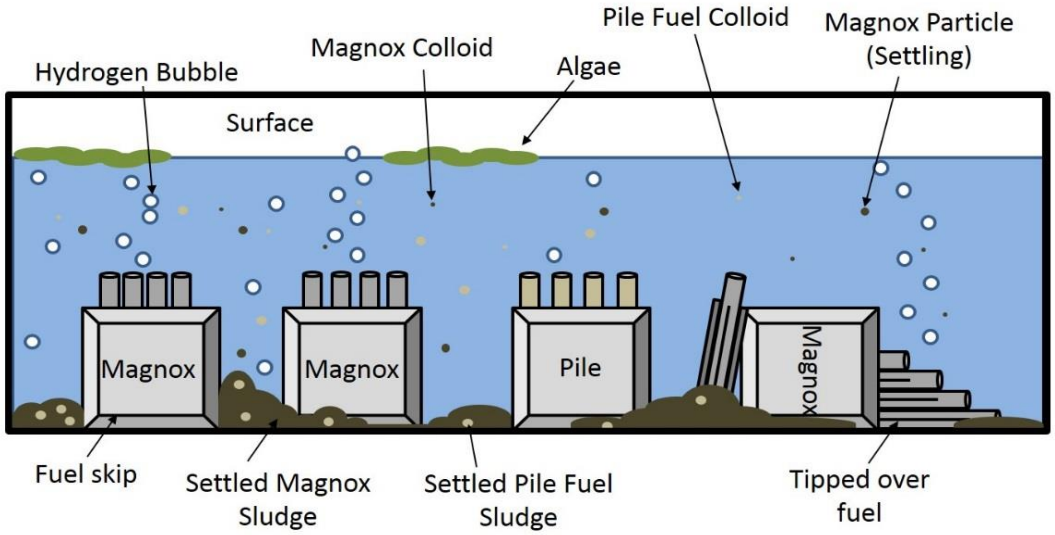

Figure 1: Illustration of the First-Generation Magnox Storage Pond with associated decommissioning challenges including the presence of corroded Magnox sludge, suspended colloidal material, corrosion driven hydrogen production, tipped fuel skips and algal contamination.

In response to these pond water treatment challenges, an aggressive sludge retrievals project has been deployed to remove as much of the sludge and other erroneous materials, to firstly reduce the challenge to SIXEP, and secondly, remove material to progress FGMSP dewatering, which is crucial for successful decommissioning[8]. In this process, $Mg(OH)_2$ sludge material is pumped at a maximum solids concentration of 2.5 vol.% using a floating platform[8]. This material is transferred at a rate of $30m^3.h^{-1}$ to an adjacent dewatering facility known as the sludge packaging plant (SPP1). In this facility, 80 m^3 batches of sludge is transferred into the three 450 m^3 tanks, when the solid sludge material sediments under gravity and the lower turbidity supernatant liquor is transferred back to FGMSP and the sludge can then packaged for final disposal when a geological disposal facility becomes available[8].

Due to wide range of particle sizes, from 6 mm uranium fuel material to nanometre scale brucite colloids known to incorporate radionuclides, sedimentation of sludge material from FGMSP may not target the smaller diameter particulates which could be returned to FGMSP in the returned supernatant, leading to downstream abatement issues[8]. Additionally, sludge dewatering is a notoriously slow process with long residence times. Research into $Mg(OH)_2$ sedimentation of similar concentrations by Johnson et al.[9] and Lockwood et al.[10] have found sedimentation rates less than 0.5 $cm.min^{-1}$. Assuming that slurry batches are consistently 2.5 vol.% solids concentration in $80m^3$ batches, it will take at least 650 sludge transfers to completely empty FGMSP of sludge[8]. In order to improve long residence times in these dewatering facilities, it is common practice to utilise polyelectrolyte macromolecules known as polymeric flocculants[11–16]. These reagents adsorb to the surface of particles and allow aggregation of smaller particulates into more settleable flocs, improving their overall sedimentation rates, which by Stokesean reasoning is a function of floc size and density[10,11,16–18].

The effectiveness of a polymeric flocculant in improving the sedimentation rate of a particulate suspension is a function of many variables. Assuming that the initial concentration of a suspension is fixed, particles are spherical and being performed in a water medium, the density of the particulates and their size are the dominating factors as per the traditional Stokes law[17,19]. However, polymeric floc structures have been investigated using techniques such as scanning election and optical microscopy are generally porous and open structures[10,20,21]. These porous structures have traditionally been modelled using fractal mathematics developed by Mandelbrot[22,23], where their structure is defined by a number known as the fractal dimension (valued between 1 and 3). Modifications have been made to Stokes law, including a dimensionless permeability number, which mathematically represents sedimentation hindrance in multiple particle settling[17]. And a fractal dimension function, which allows for a modification based on porosity which affects particle density and the effective occupied volume of the flocs from their initial flocculated state[10,12,16,24]. This has been referred to in our previous work as the fractal modified Richardson-Zaki (FMRZ) model which is described in equations 1-3. Where U_i is the zonal settling rate of a suspension, U_T is the terminal velocity of an individual floc and f_s* is dimensionless permeability number of the floc suspension. g is acceleration due to gravity, ρ_p and ρ_w are the densities of $Mg(OH)_2$ and water respectively. D_f and D_p are the diameters of a single floc and primary particles within the floc respectively, μw is the dynamic viscosity of water, d_f is the fractal dimension of the floc and ϕ_p is the volume fraction of $Mg(OH)_2$ initially in the suspension (2.5 vol.%). For polydisperse particle size distributions (PSDs), the value of $\overline{D_f}$ is problematic as it requires one particle size to be selected to represent and entire PSD. In our previous work[10], it was found the larger floc sizes, particularly those around the 90th cumulative percentile values, provided the most accurate predictions of zonal settling rate for bridging flocculation of $Mg(OH)_2$. Which was likely due to particle netting interactions as larger flocs sedimented at a greater velocity[25–27].

$$U_i = U_T \times f_s* \quad \textbf{(Eqn. 1)}$$

$$U_i = \frac{g(\rho_p - \rho_w)\overline{D_f^2}}{18\mu_w}\left(\frac{D_f}{D_p}\right)^{d_f-3} f_s^* \quad \textbf{(Eqn. 2)}$$

$$f_s* = \left(1 - \phi_p\left(\frac{D_f}{D_p}\right)^{3-d_f}\right)^{4.65} \quad \textbf{(Eqn. 3)}$$

The value of a floc structure's fractal dimension depends on the flocculation mechanism, which depends on the nature of the polymer being used[14,28–31]. Two main factors determining floc structure are the charge density and the molecular weight (MW) of the polymer[32]. Generally, there are two major electrostatically driven flocculation mechanisms, polymer bridging, and charge patch flocculation. Nominally, polymer bridging is facilitated by high MW (>10^6 g.mol^{-1}) copolymers of an ionic monomer (oppositely charged to the particle surface) and a non-ionic monomer[11,14]. Bridging flocculation polymers are referred to as statistical copolymers, which have a random configuration of comonomers, where successful bridging polymers typically have charge densities of <40 mol.% ionic comonomers[14,30]. This low charge density and high MW allows for slow polymer conformation to the particle surface, allowing the development of loops and tails, which due to segment-segment electrostatic repulsion extend out beyond the particle Debye length (electrostatic screening distance stabilising particles against spontaneous coagulation)[32]. Beyond the Debye length, they can adsorb to colliding particles producing a polymer 'bridge' between them. Bridging polymer flocs are mathematically described as having a fractal dimension < 2.1, but higher numbers have been recorded[30]. Conversely, electrostatic patch flocculation is performed with higher charge density (~100%) lower MW (~10^4-10^5 g.mol-1) homopolymers. These polymers conform quickly and tightly to a particle surface and promote flocculation by localised charge neutralisation/reversal, which reduces particle stability through Debye layer depletion and promotes agglomeration in a 'patch-wise' manner[14,32]. The resultant flocs are more densely packed and higher density than bridging flocs and usually representing with higher fractal dimensions (2.5-3)[14]. Each have different advantages; generally larger more open flocs as a result of bridging have dominant sedimentation dynamics but more susceptible to shear breakdown and cannot regrow. Whereas charge patch flocs can regrow once shear conditions are reduced but are not generally as effective at improving sedimentation in comparison[32].

In this work, the aim is to compare the performance of two different flocculants to improve SPP1 residence times. Firstly, a widely available anionic statistical copolymer flocculant, poly(acric acid)-*co*-poly(acylamide) (PAA-*co*-PAM), which was used in our previous work to improve the sedimentation dynamics of $Mg(OH)_2$ suspension[10]. Secondly, a novel amphiphilic block copolymer, consisting of two segregated homopolymer blocks of poly(acrylic acid) and poly(n-butyl acrylate), referred to hereon as PAA-*b*-PnBA. PAA-*b*-PnBA was used in our previous work as both a flocculation aid and a hydrophobising surface modifier known as a collector[33], to both flocculate $Mg(OH)_2$ and make the resultant flocs compatible with flotation operations. The aim was to use a flotation cell, which could be retrofit between FGMSP and SPP1, which would target and recover fines associated with actinide incorporation[5]. In our previous work, it was found that the longest hydrophobic chain length PAA-*b*-PnBA effectively flocculated $Mg(OH)_2$ and could remove 52 mass% of the $Mg(OH)_2$ suspension via flotation whilst retaining >80% of the water[33]. A performance which outperformed dewatering ratios by traditional collector agents used in flotation such as sodium dodecyl sulphate[15]. However, the optimum dewatering dosed concentration of PAA-*b*-PnBA for flotation performance was not the same as the optimum concentration for sedimentation, due to hydrodynamic differences between flotation and sedimentation operations. The combination of flotation and flocculation resulted in a lower volume fraction of particles post-flotation, with greater floc diameters, which by reasoning using Eqn. 1, improves zonal settling rate of the resultant suspension. To compare performance, 5 scenarios were selected and compared to see which would result in the greatest decrease in SPP1 residence time. Additionally, metrics such as final bed volume fractions were also considered. Finally, strategic caveats and future considerations, which require additional research, were discussed to help inform strategic decision making in FGMSP decommissioning when using polymeric flocculants.

SCENARIOS

Scenario 1: No polymeric flocculants are used. Dewatering is completed using only sedimentation. Shown in Fig. 2 and detailed in Table 1.

Scenario 2: Sedimentation is enhanced using 20 ppm PAA-co-PAM. Dewatering is completed using polymer aided sedimentation only. Shown in Fig. 2 and detailed in Table 1.

Scenario 3: Sedimentation is enhanced using 81 µM PAA-*b*-PnBA. Dewatering is completed using polymeric aided sedimentation only. Shown in Fig. 2 and detailed in Table 1.

Scenario 4: $Mg(OH)_2$ is flocculated using 14 µM PAA-*b*-PnBA. Dewatering is completed using polymeric aided sedimentation only. Shown in Fig. 2 and detailed in Table 1.

Scenario 5: $Mg(OH)_2$ is flocculated using 14 µM PAA-*b*-PnBA and fines removed using dispersed air flotation. The remaining cell suspension is then dewatered using polymer aided sedimentation. Shown in Fig. 2 and detailed in Table 1.

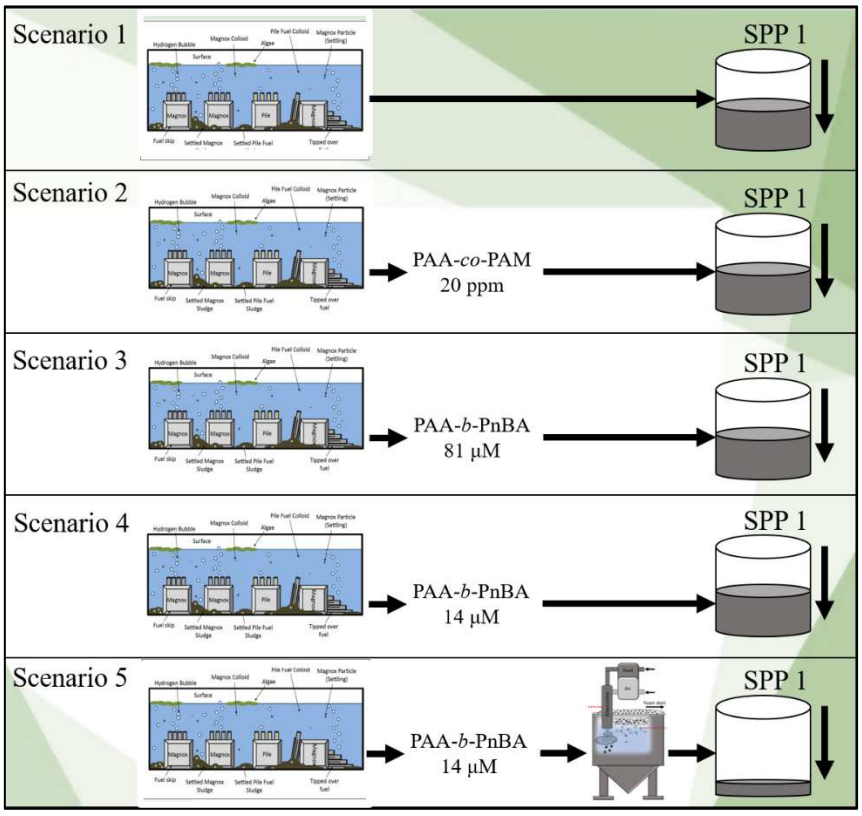

Figure 2: Diagram of Strategies 1-5.

MATERIALS & METHODOLOGY

Materials

$Mg(OH)_2$ (Versamag, Martin Marietta, US) was used for flocculation and flotation experiments and was analysed using a Malvern Mastersizer 2000E to have a particle d_{50} of 2.44 µm. Versamag is a fine white precipitated powder with a solubility of 6.9 $mg.l^{-1}$ in water[34]. Researching the same material as previous work, Lockwood et al.[35] summarised the material properties in Table 1. $Mg(OH)_2$ is made up of aggregates of pseudo-hexagonal platelets similar to those reported by Johnson *et al.* [9] and Maher *et al.*[5]. The polymers used in the study were firstly a water soluble anionic PAA-*co*-PAM copolymer, FLOPAM AN934SH (SNF® Ltd) of similar molecular weight (approximately 1.4×10^6 $g.mol^{-1}$, as provided by the supplier) with charge density 30%. 1 g of the powder provided was dissolved in 1 litre

deionised water to produce stock polymer solutions of 1000 ppm that could be sampled and diluted accordingly as in our previous work[10]. Secondly, a novel amphiphilic block copolymer PAA_{153}-*b*-$PnBA_{200}$ was synthesised using reversible addition fragmentation chain-transfer polymerisation to produce a 30 mass% copolymer solution which was diluted to form a 10000 ppm stock solution using Milli-Q water, for more details see our previous work[33]. The scenarios with their respective polymer flocculants, flocculant dose and initial solids concentration are listed below in Table 1.

Table 1: Modelled scenarios with respective polymer flocculant, flocculant dosages and initial solids concentration.

Scenario	Flocculant	Polymer dose	Initial suspension concentration	Process
1	N/A	N/A	2.5 vol.%	Settling
2	PAA-*co*-PAM	20 ppm	2.5 vol.%	Settling
3	PAA-*b*-PnBA	81 µM	2.5 vol.%	Settling
4	PAA-*b*-PnBA	14 µM	2.5 vol.%	Settling
5	PAA-*b*-PnBA	14 µM	1.4 vol.%	Flotation & settling

Floc structure characterisation

The structure of the resultant flocs in scenarios 2-5 where computed in our previous works[10,33]. The PAA-*co*-PAM polymer in scenario 2 had a more open floc structure displaying fractal dimensions of 2.07 and minimum repeating floc sizes and primary particle sizes of 6.74 and 0.28 µm respectively resulting a in a solid volume fraction of 3.4%[10]. For scenarios 3, 4 and 5, floc structure varies with different PAA-*b*-PnBA concentrations. For scenario 3, with a PAA-*b*-PnBA concentration of 81 µM the resultants flocs displayed fractal dimensions of 2.38, densities of 1238 $kg.m^{-3}$ and minimum repeating floc sizes and primary particle sizes of 1.68 and 0.16 µm respectively. For scenarios 4 and 5, with a PAA-*b*-PnBA concentration of 14 µM the resultants flocs displayed fractal dimensions of 2.29, densities of 1236 $kg.m^{-3}$ and minimum repeating floc sizes and primary particle sizes of 1.26 and 0.17 µm respectively. The dimensionless permeability number of scenarios 2-4 can be calculated using Eqn. 3. For scenarios 2, 3 and 4/5, the dimensionless permeability numbers are calculated from data in Tables 1 and 2 and are 0.05, 0.58, 0.6 and 0.75 respectively.

Table 2: Floc structure variables for scenarios 2-4 showing the fractal dimension, d_f, minimum repeating floc diameter, D_f, primary particle size, D_p, the floc density, ρ_f and the dimensionless permeability number f_s.*

Variable	Scenario 2	Scenario 3	Scenario 4	Scenario 5
d_f	2.07	2.38	2.29	2.29
D_f [µm]	6.74	1.68	1.26	1.26
D_p [µm]	0.28	0.16	0.17	0.17
ρ_f [$kg.m^{-3}$]	1045	1238	1236	1236
f_s*	0.05	0.58	0.60	0.75

Sedimentation analysis and settled bed concentration

Sedimentation was analysed for the statistical and block copolymers in 2 differing ways as a function of available copolymer. The PAA-*co*-PAM system analysed in our previous work[10] for scenario 2 were prepared in a 1 litre reactor vessel 25 cm in diameter with four baffles and mixed using a four-blade axial flow impeller of 50 mm diameter, and 60° pitch, which was located 2 cm from the base of the reactor vessel. Impeller rotation rate was at 300 rpm, as this was determined to be a sufficient agitation

rate to keep flocs suspended and prevent sedimentation, while reducing shear degradation experienced with higher mixing rates. The required polymer was then added in 5 ml aliquots via a calibrated micropipette over a period of no more than 10 seconds at the centre of the suspension, to ensure an even distribution throughout the system. Visual observation of suspension-supernatant boundary level change with time was used to measure the influence of polymer concentration on hindered settling rates. Flocculated suspensions were then transferred to 1 litre measuring cylinders of 61 mm diameter. The cylinders were inverted 5 times to evenly re-suspend flocs and the interfacial height was measured over time. Whereas the sedimentation analysis for the PAA-*b*-PnBA system was completed by stirred using a magnetic stirring a 250 ml 2.5 vol% $Mg(OH)_2$ suspension at 400 rpm for 10 mins to ensure an even suspension of $Mg(OH)_2$. Given volumes of the chosen polymer stock solution were then added to the beaker which continued to be stirred at 400 rpm for a further 20 mins. Turning the stirrer off and removing the magnetic stirrer bar, the solution was then poured into a volumetric cylinder (100 mL). Waiting for the mudline to appear and fall, a stopwatch was used to measure the time taken for the mudline to fall from the 80 ml to 60 ml mark on the measuring cylinder, as shown by the photograph of the experiment set up in Fig. 3. The settled bed concentration was determined by allowing the flocculated and raw suspensions to settle for 48 hours then the final solids concentration was recorded.

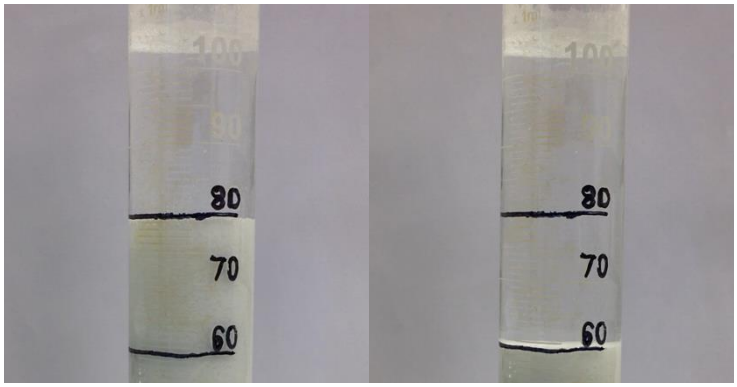

Figure 3: Photograph taken of the set up for batch settling rate experiments in a 100 mL volumetric cylinder, showing the fall of the mudline over time.

RESULTS, DISCUSSION AND IMPLEMENTATION CONSIDERATIONS

-Scenario 4 and 5 floc size characterisation

The structural differences between scenarios 2-5 are a function of the both the polymer and polymer dosages used. Firstly, for the PAA-*co*-PAM used in Scenario 2, both floc density and the fractal dimension were lower than the other polymer driven dewatering strategies in Scenarios 3-5. This is commonly observed when using lower charge density higher molecular weight polymers to flocculate counter-ionically charged particles[13]. The slower conformation of the polymer chains onto the surface of the $Mg(OH)_2$ results in greater loops and tails which extend beyond the Debye layer[32]. Additionally, the process of adsorption of anionic functional groups onto the cationic particle surface reduces the ionic strength of the particle and thus the extent of the Debye layer[11]. These loops and tails result in more open structures and thus lower densities commonly observed in bridging flocculation. This was also observed using cryogenic scanning electron microscopy in our previous work[10]. Scenarios 3-5 utilised the PAA-*b*-PnBA polymer. In our previous work[33], Scenario 3 utilised a concentration of 81 µM, this concentration was associated with a multi-layer adsorption mechanism[33]. Scenario 4 and 5 which utilised PAA-*b*-PnBA concentrations of 14 µM are assumed structurally identical. Our previous work indicated that the adsorption regime utilised at this concentration was monolayer. Interestingly there wasn't a notable difference in floc density between Scenarios 3-5 although their fractal dimensions were different, with Scenario 3 displaying a fractal dimension of 2.38 whereas Scenarios 4 & 5 had fractal dimensions of 2.29. It was suggested that because amphiphilic block copolymers such as PAA-

b-PnBA form pre-micellular aggregates which have an affinity for the $Mg(OH)_2$ surface likely resulting in a structural transition to a more open structure, utilising a combination of charge patch, charge neutralisation and hydrophobic interactions to facilitate flocculation. However, due to the highly hydrophobic nature of the non-ionic PnBA chain segment, some floc contraction and densification may be occurring with increasing surface coverage due to entropically driven water liberation form the floc[36]. In our previous work, Scenario 4 was analysed using single-element optical microscopy, the particle size distribution pre-flotation is shown below in Fig. 3, the d_{10}, d_{50} and d_{90} values were found to be 136 µm, 390 µm and 804 µm respectively. Post-flotation there was a lower d_{90} reported (660 µm) indicating that the flotation process was hydrodynamically hindered[33].

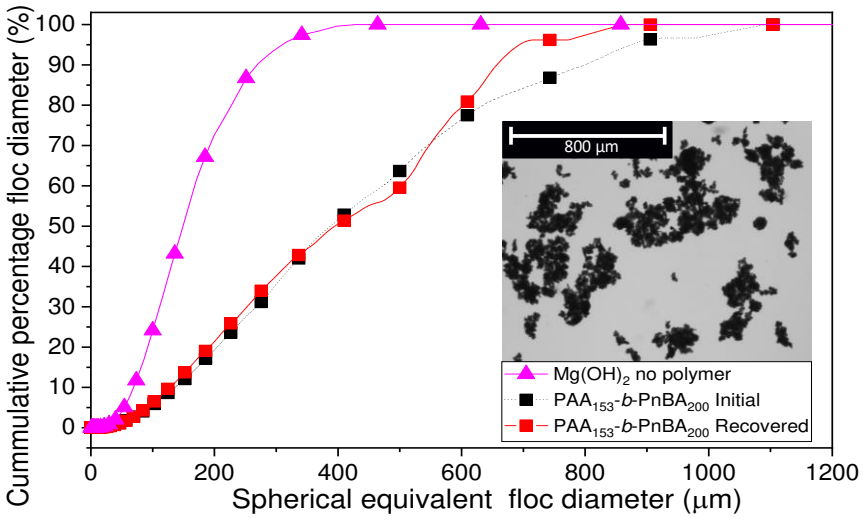

Figure 3: Spherical equivalent floc size cumulative frequency distribution of Scenarios 1 and 4, using single-element optical microscopy and floc micrographs from Scenario 4.

-Scenario 5 sedimentation model selection and validation

The selection of sedimentation models for predicting zonal rates is vital in being able to decide residence times for sludge batches sent from FGMSP to SPP1. Whilst work has been completed in acoustic backscatter to help monitor sedimentation[16], more work is required in understanding the sedimentation dynamics of these suspensions, especially when considering $Mg(OH)_2$ flocculated with polymers which aggregate particles by different flocculation mechanisms. For example, because of the greater effective suspension volume due to the lower fractal dimension flocs facilitated using the statistical copolymer PAA-*co*-PAM, there is a lower dimensionless permeability number (see Table 2) for scenario 2 than in Scenarios 3-5. It was established in our previous work[10] that this increasing in effective floc volume meant that inter-aggregate packing approach intra-aggregate packing and there was significant particle interactions. Larger flocs mostly influenced the sedimentation rate and the reduction in inter-aggregate spacing allowed an assumption that drag effects and shape effects would be negligible and that there was likely significant flow through the flocs porous structure[10,12]. Using the experimentally determined zonal settling rates in Scenario 4, recorded size data in Fig. 3 was used to firstly determine appropriate sedimentation models which could be used to estimate SPP1 residence times and secondly determine which size data was appropriate to represent a polydisperse suspension. Previously, Vahedi and Gorczyca[37] suggested a terminal settling velocity relationship shown in Eqn. 4 which incorporates a drag coefficient, which is a function of the particle Reynolds number, *Re,* shown in Eqn. 5. Hereon Eqn. 4 will be referred to as the DRAG model and Eqn. 2 as the FMRZ model. Additionally, Vahedi and Gorczyca[37] include a non-sphericity factor, η, which is a function of the floc aspect ratio, however due to high aspect ratios of ~0.7 indicating near sphericity for more open floc structures found in our

previous work[10], η is assumed to be 1. Previous work by Paul et al.[38]found when investigating the sedimentation of Caesium phosphomolybdate, zirconium molybdate and zirconium citromolybdate displaying spheroidal, cubic and rectangular cuboidal morphologies respectively, the Richardson-Zaki (RZ) exponent, n in Eqn. 4, was greater than 4.65 due to shape induced drag.

$$U_i = \frac{\eta(\rho_p - \rho_w)g}{18\mu_w} D_p^{3-d_f} \frac{\overline{D_f}^{d_f-1}}{1+0.15Re^{0.687}} \left(1 - \Phi_p \left(\frac{D_f}{D_p}\right)^{3-d_f}\right)^n \quad \textbf{(Eqn. 4)}$$

$$Re = \frac{U_T \overline{D_f} \rho_w}{\mu_w} \quad \textbf{(Eqn. 5)}$$

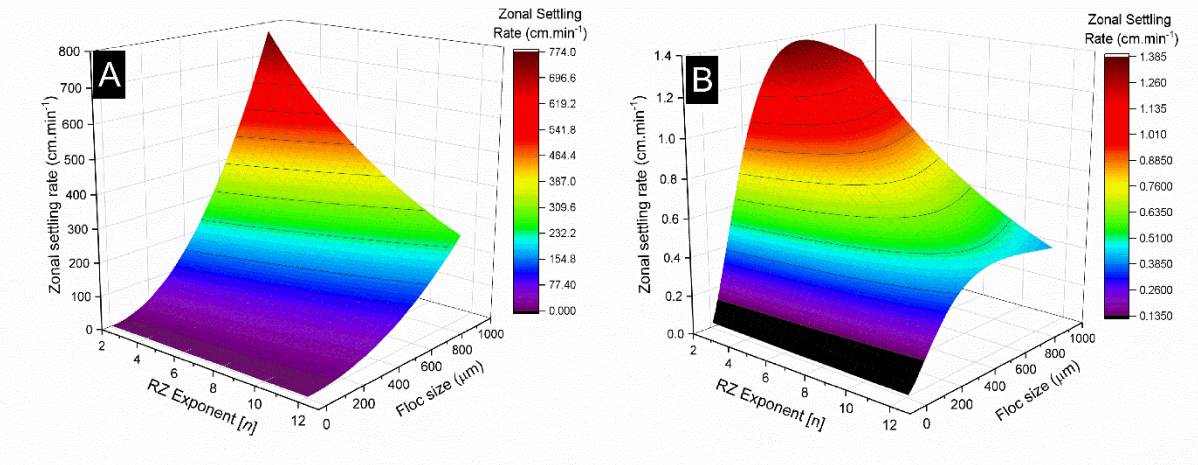

Figure 4: Multivariate analysis of A) Fractal modified Richardson-Zaki (FMRZ) settling model shown in Eqn. 2 and B) drag-modified FMRZ (DRAG) settling model shown in Eqn. 4, which are used to predict sedimentation rates of 2.5 vol% $Mg(OH)_2$ flocculated using 14 µM Poly(acrylic acid)-block-poly(n-butyl acrylate)[see scenario 4]. Here the sensitivity of zonal settling rate was investigated by varying the polydisperse floc size, $\overline{D_f}$, and the Richardson-Zaki (RZ) exponent, n. Where ρ_p= 2340.6 kg.m^{-3}, ρ_w= 1000 kg.m-3, μ_w= 8.9 × 10-4 kg.m^{-1}.s^{-1}, D_f=1.26 µm and D_p= 0.17 µm.

A multivariate analysis was performed probing the FMRZ and DRAG model's sensitivity to polydisperse floc size (0-1000 µm) and the RZ-Exponent (2-12) shown in Fig. 4A and 4B respectively. There are marked differences between the two models, where the FMRZ model in Fig 4A shows a drastic increase in zonal settling rate over the same polydisperse floc size and RZ-exponent range. The distinct difference between the two models is that the DRAG model, by definition, incorporates a drag coefficient which is a function of the non-linear reciprocal of floc diameter. This drag coefficient, d_c, is proportional to the particle Reynolds number where $U_i \propto d_c \propto \frac{1}{1+0.15Re^{0.687}}$ and $Re \propto \overline{D_f}$. This non-linear reciprocal relationship between zonal settling rate and polydisperse floc size means that zonal settling rate increases initially with increasing floc diameter. Then as boundary layer separation occurs when the inertia of the fluid begins to dominate settling dynamics, the floc size increase begins to inhibit zonal settling rate[17,39]. This limits the zonal settling rate to >1.5 cm.min^{-1} rather than increasing indefinitely. Additionally, the effect of increasing RZ-exponent further inhibits the zonal settling rate as it is order unity to the power of increasing exponent values, models the increasing hindered drag and shape effects in hindered settling regimes observed by Paul et al.[38].

Table 3: Experimentally and modelled polydisperse floc diameters using the fractal modified Richardson-Zaki (FMRZ) settling model and the drag-modified FMRZ (DRAG) settling model, using experimentally determined zonal settling rates and various RZ-exponent (n) inputs.

System	Zonal settling rate [U_i]	Polydisperse floc diameter [$\widetilde{D_f}$]
Experimentally determined d_{50}	1.33	390 µm
FMRZ model (Eqn. 2), n=4.65	1.33	43 µm
DRAG model (Eqn. 4), n=4.65	1.33	328 µm
DRAG model (Eqn. 4), n=6.52	1.33	390 µm
DRAG model (Eqn. 4), n=13.77	1.33	804 µm

Scenario 5 post-flotation sedimentation modelling

To validate which model is more representative of Scenario 4, the FMRZ and DRAG models where compared in Table 3, which uses the experimentally measured sedimentation rate of Scenario 4, U_i = 1.33 ± 0.06 cm.min^{-1}, to calculate the polydisperse floc diameters using the FMRZ and DRAG models. These were then compared to the measured d_{50} and d_{90} polydisperse floc diameters in Fig. 3. Notably when using the FMRZ model assuming the linear spherical RZ-exponent, n = 4.65, the computed polydisperse floc diameter was significantly lower than the experimentally determined d_{50} and d_{90} Scenario 4 values at ~43 µm. The diameter was computed iteratively using the DRAG model approximating a polydisperse floc diameter of ~328 µm which more closely reflected experimentally determined floc diameters in Fig. 3, specifically Scenario 4s d_{50}. As the DRAG model appeared to be more likely to give a good first approximation of sedimentation rates in Scenario 4 and thus more accurate modelled Scenario 5 zonal settling rates, the experimentally determined d_{50} and d_{90} values in Fig. 3 were used to compute the RZ-exponent iteratively using the experimentally determined zonal settling rates. This computed RZ-exponents of 6.52 and 13.77 for the d_{50} and d_{90} values respectively shown in Table 3. Whilst greater than the linear sphericity RZ-exponent, similar RZ-exponents were reported by Johnson et al.[9] and Paul et al.[38] in hindered sedimentation work. The selection of model inputs are complex, when investigating Scenario 2 in our previous work[10], the FMRZ model required an input of the d_{90} floc size to produce first approximation of sedimentation rate. It was argued that because of the lack of inter-aggregate spacing computed form the low dimensionless permeability number, that particle interactions were not negligible and that larger flocs dominate the sedimentation rate. Larger flocs may encompass smaller flocs as they settle at a greater rate similar to what is observed in sweeping flocculation systems[10]. However, in this system, because interaggregate spacing is greater, these particle interactions may be less prominent. It should be noted that the block copolymer flotation process in our previous work[33] (shown in Fig. 3) was found to target fine material and was hydrodynamically limited prohibiting the flotation of larger floc sizes >660 µm. This implies that larger floc sizes may be more appropriate for modelling post-flotation sedimentation rates.

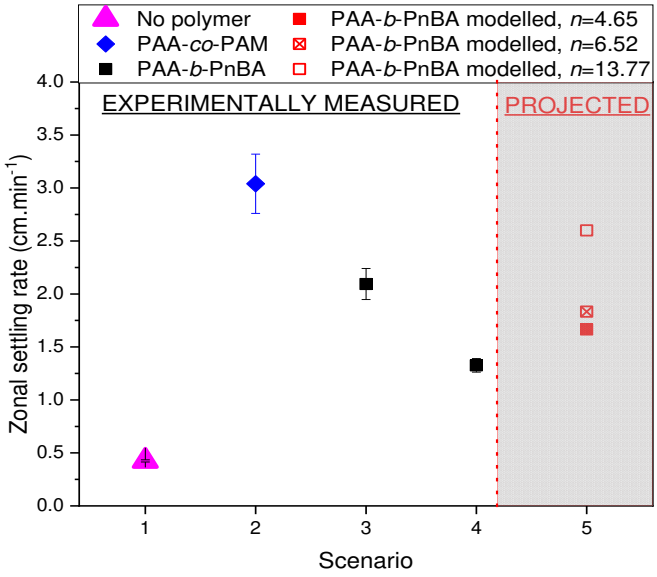

Figure 5: Scenarios 1-5 with their corresponding zonal settling rates.

The predicted zonal settling rate for Scenario 5 was modelled by taking the experimentally determined zonal settling rate, $U_{i.s4}$ = 1.33 ± 0.06 cm.min^{-1}, and applying the functional permeability number proportionalities shown in Eqn. 6, where $\Phi_{p.s4}$ & $\Phi_{p.s5}$ are the solid volume fractions for scenario 4 (0.025) and 5 (0.014) respectively. The RZ-exponent, n, was varied between 4.65, 6.52 and 13.77 to reflect the use of the linear spherical assumption and the experimentally determined d_{50} and d_{90} values used as inputs respectively. Interestingly, the increase in RZ-exponent value increases the predicted zonal settling rate, where the use of the d_{90} floc size (804 µm) and n=13.77 predicts the greatest zonal settling rate of 2.6 cm.min^{-1}.

$$U_{i.S5} = U_{i.S4} \times \frac{\left(1-\Phi_{p.S5}\left(\frac{D_f}{D_p}\right)^{3-d_f}\right)^n}{\left(1-\Phi_{p.S4}\left(\frac{D_f}{D_p}\right)^{3-d_f}\right)^n} \quad \textbf{(Eqn. 6)}$$

Comparing zonal settling rates, Scenarios 1-4 are experimentally determined whereas Scenario 5 is modelled based on FMRZ and DRAG models. Fig. 5 shows that all Scenarios 2-5 display a greater zonal settling rate than Scenario 1, where Scenario 1 represents the $Mg(OH)_2$ sedimentation rate without the aid of polymeric flocculants and displays a sedimentation rate of 0.42 cm.min^{-1}. Scenario 2, which utilises the statistical copolymer PAA-*co*-PAM, produces the greatest zonal settling rate of the 5 scenarios with a sedimentation rate of 3.04 cm.min^{-1}. Comparing Scenarios 3 and 4, the greater concentration of the amphiphilic block copolymer, PAA-*b*-PnBA, produced larger flocs which were more compact with a fractal dimension of 2.38 for scenario 3 (81 µM), whereas the lower concentration used in scenario 4 (14 µM) has a lower fractal dimension of 2.29, indicating more open structured flocs. The average densities of flocs in scenarios 3 and 4 are effectively identical as shown in Table 2. The greater the concentration of PAA-*b*-PnBA, the greater the zonal settling rate of the suspension (scenario 3 = 2.09 cm.min^{-1} and scenario 4 = 1.33 cm.min^{-1}), which is linked to the greater floc sizes associated with an increase in polymer concentration given the consistent floc densities with polymer dose. Scenario 5 shows an increased sedimentation rate, which is attributed to the modelled increase in the functional permeability number, due to a decrease in the solid suspension concentration thus reducing hindering effects post-flotation. Given the issues associated with selecting a single floc size to represent an entire polydisperse floc population, it is likely that the appropriate polydisperse floc size lays between the d_{50} and d_{90} flocs size. Volume weight mean diameters, or De Brouckere mean diameter ($d_{[4,3]}$), are often quoted as being an appropriate floc size to represent the floc population[40], which is

calculated using Eqn. 7 computing a $d_{[4,3]}$ size of 573 µm. Using the DRAG model, the RZ-exponent was calculated as n=10.51. Using Eqn. 6, the $d_{[4,3]}$ zonal settling rate post-flotation was predicted as 2.23 cm.min^{-1}. Ultimately, whilst there is some uncertainty as to the degree of increase in zonal settling rate post-flotation, there is high confidence that the zonal settling rate is likely between 1.66-2.6 cm.min^{-1}.

$$d_{[4,3]} = \frac{\int_0^1 \overline{D_f}^4 dF_n}{\int_0^1 \overline{D_f}^3 dF_n} = \frac{\sum f_{n.i} \overline{D_{f.i}}^4}{\sum f_{n.i} \overline{D_{f.i}}^3} \quad \textbf{(Eqn. 7)}$$

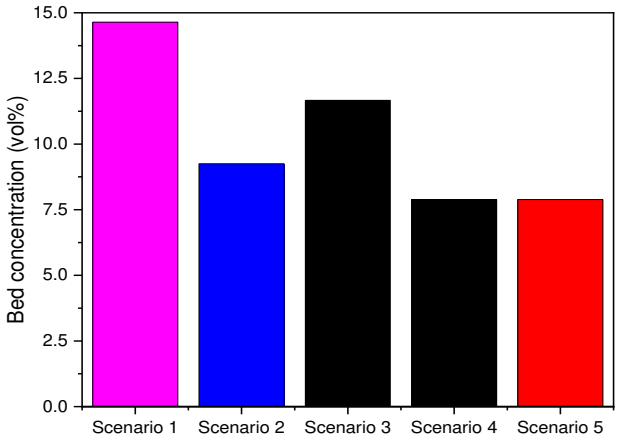

Figure 6: Settled bed concentrations for each of the 5 experimentally determined and modelled dewatering scenarios for sludge packaging plant 1.

Comparing settled bed concentrations of the 5 scenarios, it is clear from Fig. 6, that the application of polymeric flocculants decreases the consolidated bed concentrations. Interestingly, there is a marked difference between Scenarios 3 & 4/5, where Scenario 5 is assumed to be of equal concentration to Scenario 4 but only 48% of the final volume post-flotation. Scenario 3 has a greater bed concentration than Scenario 4, which is likely a reflection of the structural and flocculation mechanistic differences which is a function of concentration. However, an investigation by O'Shea et al.[41] found when investigating statistical copolymers of PAA and PNIPAM, where PNIPAM is temperature sensitive. At 50°C, the polymer was hydrophobic and facilitated flocculation. At 25°C, the polymer had a much more consolidated bed than when heated to 50°C, which was due to the increased mechanistic strength provided by the particle-particle attraction resisting the downward weight of the sediment bed. This relationship was also observed by Franks[42] when investigating pH sensitive polymers such as chitosan which became hydrophobic at greater pH's promoting flocculation, then by reducing the pH became repulsive allowing beds to consolidate further. In this system where the opposite is observed, it is likely that due to the multilayer adsorption, there is a high degree of hydrophobic water liberation from the settled floc structures. A previous investigation by Volpert et al.[36] of adsorption of amphiphilic block copolymers onto clay surfaces found that highly hydrophobic adsorbed layers would liberate water almost completely from particle surfaces depending on the comonomer functional group hydrophobicity. This implies that there could be floc contraction with increasing PAA-*b*-PnBA adsorption in the multilayer regime as water may be liberated from the structure, increasing floc density and reducing bed volumes. Additionally, the molecular weight of the PAA-*b*-PnBA is substantially lower (~10^4 g.mol^{-1}) than those investigated by O'Shea et al.[41] and Franks.[42] (~10^6 g.mol^{-1}). Where the latter work used polymers associated with bridging flocculation and reported substantially lower surface adsorption when compared with PAA-*b*-PnBA in this work[33]. It has been observed by Avadiar et al.[43] that there is a relationship between polymeric flocculant molecular weight (but more specifically the

flocculation mechanism) and the resultant yield stress of sedimented beds which display non-Newtonian behaviour. The larger molecular weight polymers utilised a bridging flocculation mechanism produced a complex network, where this interlinking network produced the increased yield stress, this observation has also been linked to the bed resistance to consolidation by O'Shea et al.[41].

There are many factors to consider when selecting which scenario is optimum for site operation and additional considerations must be made outside the scope of this investigation. Whilst improving the sedimentation rate of the flocculated suspensions is important to reduce residence times and total operation time, the resultant bed solid volume fraction is an important consideration. Whilst reducing bed volumes directly influences the amount of waste required to be dedicated to a geological waste disposal facility, the sedimented sludge must be further processed, which includes transport from SPP1[8]. Given multiphase transport is further complicated by nuclear industrial environments, where blockages and pump failures can be orders of magnitude more difficult to address, the settled flocculated sludge rheology in this intermediate stage is an important consideration and the resultant bed yield stresses of these systems should be addressed in future work. Additionally, there are other caveats which should be considered when proposing the discussed technologies in this work. Whilst flotation has several deployability advantages including low geographical footprint requirements (Jameson flotation cell tank diameters can be as small as 0.19 m^2 and other designs are even mobile[44]), no moving parts inside the tank as well as a notable chemical robustness to variable feed compositions[45,46], aerosolization of radionuclides is a possibility and may require more robust engineering solutions such as implementation of HEPA filters. The foam phase of flotation will not only have a lower water content due to air bubbles meaning gamma ray shielding would need to be considered, but this scenario requires the design of an additional radwaste stream. The resilience of polymeric flocculants to alpha and beta radiation from the embedded radionuclides on the $Mg(OH)_2$ surface in real sludge should also be considered[5]. Particularly the potential environmental chemistry of the radiolytic degradation products, to ensure they do not facilitate radioisotope mobility in geological disposal facilities. Whilst there are many uncertainties that require investigation, polymeric flocculants have shown to be very effective and economical tools to improve and aid in dewatering of these self-confessed intolerable risk facilities at Sellafield site.

CONCLUSIONS

5 hypothetical scenarios were analysed and modelled to compare the deployment of two different polymers to improve the dewatering of a nuclear fuel storage pond, where one scenario incorporated flotation to first remove some material prior to sedimentation, specifically the fines. Polymeric flocculants were shown to be effective at increasing zonal settling rates of a radwaste simulant based on corroded Magnox fuel cladding. The large molecular weight, bridging mechanism flocculant, PAA-*co*-PAM, was more effective at improving zonal settling rates. This was due to their large open structure flocs compared to lower molecular weight, PAA-*b*-PnBA, diblock polymer alternative. PAA-*b*-PnBA was found to produce denser flocs than the PAA-*co*-PAM system, which remained constant with increasing floc size. As the PAA-*b*-PnBA flocs were much more compact, the greater inter-aggregate spacing compared to the PAA-*co*-PAM system meant that drag effects had to be incorporated into an established fractal-modified Richardson-Zaki sedimentation model to accurately predict zonal settling rates and floc diameters. The modelled post-flotation scenario had imbedded uncertainty due to the polydispersity of the particle size distribution, however, the performance post-flotation was greater than pre-flotation. The resultant bed concentrations showed that the PAA-*co*-PAM system displayed documented resistance to compression due to the complex interlinking particle network providing additional mechanical strength. The PAA-*b*-PnBA system with more compact flocs also produced the most compact bed at its optimum sedimentation concentration. Further work is required to underpin the optimum scenario to implement to most effective settling aid to sediment Magnox radwaste, especially regarding settled bed rheology, which may affect downstream operations and result in particulate resuspension.

ACKNOWLEDGEMENTS

The authors would like to thank the Engineering and Physical Sciences Research Council (EPSRC) U.K and Sellafield Ltd for funding this research through the Centre for Doctoral training in Next Generation Nuclear (NGN-CDT) [EP/L015390/1].

REFERENCES

1 S. F. Jackson, S. D. Monk and Z. Riaz, *Appl. Radiat. Isot.*, 2014, **94**, 254–259.

2 K. R. Hallam, P. C. Minshall, P. J. Heard and P. E. J. Flewitt, *Corros. Sci.*, 2016, **112**, 347–363.

3 Department for Business Energy and Industrial Strategy, *2019 UK Radioactive Waste Detailed Data*, 2019.

4 A. Richardson and P. Maher, Sellafield Fuel Handling Plant Pondwater update NuSAC(04)P17. (Update of NuSAC(03)P10), http://www.hse.gov.uk/aboutus/meetings/iacs/nusac/051104/p10.pdf, (accessed 16 June 2018).

5 Z. Maher, P. Ivanov, L. O'Brien, H. Sims, R. J. Taylor, S. L. Heath, F. R. Livens, D. Goddard, S. Kellet, P. Rand and N. D. Bryan, *J. Nucl. Mater.*, 2016, **468**, 84–96.

6 K. S. Leonard, D. McCubbin and M. B. Lovett, *Sci. Total Environ.*, 1995, **175**, 9–24.

7 R.-M. Woods and M. E. Gunter, *Am. Mineral.*, 2001, **86**, 424–430.

8 I. Grant, U. Weintrager, I. E. Richardson and D. Wilson, in *Waste Management Symposium*, Phoenix, Arizona, USA, 2016.

9 M. Johnson, J. Peakall, M. Fairweather, S. Biggs, D. Harbottle and T. N. Hunter, *I&EC Res.*, 2016, **55**, 9983–9993.

10 A. P. G. Lockwood, J. Peakall, N. J. Warren, G. Randall, M. Barnes, D. Harbottle and T. N. Hunter, *Chem. Eng. Sci.*, 2020, 116274.

11 M. S. Nasser and A. E. James, *Sep. Purif. Technol.*, 2006, **52**, 241–252.

12 A. R. Heath, P. A. Bahri, P. D. Fawell and J. B. Farrow, *AIChE J.*, 2006, **52**, 1987–1994.

13 Y. Zhou and G. V. Franks, *Langmuir*, 2006, **22**, 6775–6786.

14 G. V Franks, P. D. Yates, N. W. A. Lambert and G. J. Jameson, *Int. J. Miner. Process.*, 2005, **77**, 46–52.

15 A. P. G. Lockwood, P. Kok Shun, N. Basharat, T. Barber, J. Peakall, N. Warren, G. Randall, M. Barnes, D. Harbottle and T. Hunter, *RSC Adv.*

16 T. N. Hunter, J. Peakall, D. Egarr, D. M. J. Cowell, S. Freear, A. S. Tonge, L. Horton, H. P. Rice, I. Smith, K. Malone, D. Burt, M. Barnes, G. Randall, S. Biggs and M. Fairweather, *Chem. Eng. Sci.*, 2020, **218**, 115560.

17 M. Rhodes, *Introduction to Particle Technology : Martin J. Rhodes*, Wiley, 2008.

18 H. Li, J.-P. O'Shea and G. V. Franks, *AIChE J.*, 2009, **55**, 2070–2080.

19 J. F. Richardson and W. N. Zaki, *Trans. Instn. Chem. Engrs.*, 1954, **32**, 35–53.

20 D. Sharma, S. Lin, C, Miller, J, *Miner. Eng.*, 2017, **101**, 20–29.

21 A. Vahedi and B. Gorczyca, *Water Res.*, 2011, **45**, 545–556.

22 B. B. Mandelbrot, *The fractal geometry of nature*, W.H. Freeman, 1982.

23 B. B. Mandelbrot, *Fractals : form, chance, and dimension*, W.H. Freeman, 1977.

24 A. Khelifa and P. S. Hill, *J. Hydraul. Res.*, 2006, **44**, 390–401.

25 B. Shi, Q. Wei, D. Wang, Z. Zhu and H. Tang, *Colloids Surfaces A Physicochem. Eng. Asp.*, 2007, **296**, 141–148.

26 P. Jarvis, B. Jefferson and S. A. Parsons, *Water Res.*, 2006, **40**, 2727–2737.

27 D. Ghernaout and B. Ghernaout, *Desalin. Water Treat.*, 2012, **44**, 15–28.

28 C. M. Sorensen, *Aerosol Sci. Technol. Am. Assoc. Aerosol Res.*, 2001, **35**, 648–687.

29 F. Pierce, C. M. Sorensen and A. Chakrabarti, *Phys. Rev. E*, 2006, **74**, 021411.

30 G. C. Bushell, Y. D. Yan, D. Woodfield, J. Raper and R. Amal, *Adv. Colloid Interface Sci.*, 2002, **95**, 1–50.

31 T. G. M. Van De Ven, *Adv. Colloid Interface Sci.*, 1994, **48**, 121–140.

32 J. Gregory and S. Barany, *Adv. Colloid Interface Sci.*, 2011, **169**, 1–12.

33 A. Lockwood, G. Wadsley, N. Warren, D. Harbottle, T. Hunter, J. Peakall, G. Randall and M. Barnes, in *Waste Management Symposium 2020*, Phoenix, Arizona, USA., 2020.

34 Martin Marietta Magnesia Specialties, *Fed. Regist.*, 2016, **77**, 1–7.

35 A. P. G. Lockwood, P. Kok Shun, D. Harbottle, N. J. Warren, G. Randall, J. Peakall and T. N. Hunter, in *Waste Management Symposium*, Phoenix, Arizona, USA, 2019.

36 E. Volpert, J. Selb, F. Candau, N. Green, J. F. Argillier and A. Audibert, *Langmuir*, 1998, **14**, 1870–1879.

37 A. Vahedi and B. Gorczyca, *Water Res.*, 2014, **53**, 322–328.

38 N. Paul, S. Biggs, J. Shiels, R. B. Hammond, M. Edmondson, L. Maxwell, D. Harbottle and T. N. Hunter, *Powder Technol.*, 2017, **322**, 75–83.

39 J. Peakall, J. Ashworth, P. Best, in *The scientific nature of geomorphology : proceedings of the 27th Binghamton Symposium in Geomorphology*, ed. L. Thorn, C, E. Rhoads, B, Wiley, New York, 1996, pp. 221–253.

40 J. Peakall, J. Ashworth, P. Best, in *The scientific nature of geomorphology : proceedings of the 27th Binghamton Symposium in Geomorphology*, ed. L. Thorn, C, E. Rhoads, B, Wiley, New York, 1996, pp. 221–253.

41 J. P. O'Shea, G. G. Qiao and G. V. Franks, *J. Colloid Interface Sci.*, 2010, **348**, 9–23.

42 G. V. Franks, *J. Colloid Interface Sci.*, 2005, **292**, 598–603.

43 L. Avadiar, Y. K. Leong and A. Fourie, *Powder Technol.*, 2014, **254**, 364–372.

44 H. B. Ortiz-Oliveros and R. M. Flores-Espinosa, *Process Saf. Environ. Prot.*, 2020, **144**, 23–31.

45 G. Harbort, S. De Bono, D. Carr and V. Lawson, *Miner. Eng.*, 2003, **16**, 1091–1101.

46 D. Osborne and J. Euston, *Independent Report Value of the Jameson Cell to the Australian Economy Contents*, Wellington point, Australia, 2015.